J Intell Robot Syst (2012) 68:275–291
DOI 10.1007/s10846-012-9677-6

Upper-Limb EMG-Based Robot Motion Governing Using Empirical Mode Decomposition and Adaptive Neural Fuzzy Inference System

Hsiu-Jen Liu · Kuu-Young Young

Received: 31 March 2011 / Accepted: 30 April 2012 / Published online: 22 May 2012

Abstract To improve the quality of life for the disabled and elderly, this paper develops an upper-limb, EMG-based robot control system to provide natural, intuitive manipulation for robot arm motions. Considering the non-stationary and nonlinear characteristics of the Electromyography (EMG) signals, especially when multi-DOF movements are involved, an empirical mode decomposition method is introduced to break down the EMG signals into a set of intrinsic mode functions, each of which represents different physical characteristics of muscular movement. We then integrate this new system with an initial point detection method previously proposed to establish the mapping between the EMG signals and corresponding robot arm movements in real-time. Meanwhile, as the selection of critical values in the initial point detection method is user-dependent, we employ the adaptive neuro-fuzzy inference system to find proper parameters that are better suited for individual users. Experiments are performed to demonstrate the effectiveness of the proposed upper-limb EMG-based robot control system.

Keywords Electromyography (EMG) · Human-assisting robot · Upper-limb motion classification · Empirical mode decomposition (EMD) · Adaptive neuro-fuzzy inference system (ANFIS)

K.-Y. Young (✉)
Department of Electrical Engineering,
National Chiao Tung University,
1001 University Road, Hsinchu 300, Taiwan
e-mail: kyoung@mail.nctu.edu.tw

H.-J. Liu
National Space Organization,
8F, 9 Prosperity 1st Road, Hsinchu Science Park,
Hsinchu 30078, Taiwan
e-mail: hank@nspo.narl.org.tw

1 Introduction

Electromyography (EMG) signals, generated during muscle contraction, in some sense reflect human intentions. Therefore, some research has focused on the study of using EMG signals to control rehabilitation devices [1–4] and human-assisting manipulators [5–10], so that the physically handicapped as well as the elderly may use them to improve their mobility and quality of life. However, since nonlinear, non-stationary characteristics and high variations are inherently present in EMG signals, these disturbances make it hard to analyze and discriminate among EMG signals. Consequently, figuring out how to achieve a high discrimination rate for EMG pattern recognition still remains a challenge. Several methods for recognizing the intended movements from EMG signals have been proposed. In the time domain, there are mean absolute value, variance, bias

zero-crossing, Willison amplitude, AR-model [1, 2, 11], Euclidean distance and standard deviation [12], and hidden Markov model [13], etc. In the frequency domain, there are Fourier transform [14] and wavelet analysis [15, 16], etc. Unfortunately, the time-domain approaches usually include high computational complexity [2]. As for approaches in frequency domain, the data must be linear and strictly stationary for Fourier transform [17] to work; however, EMG signals are nonlinear and non-stationary signals, especially for contraction levels higher than 50% of maximum voluntary contraction [18]. Meanwhile, a mother wavelet has to be defined a priori for wavelet analysis [19]. Unsuitable mother wavelets may lead to unsatisfactory results.

In contrast, Hilbert–Huang transform (HHT) is a time-frequency method. Based on the local time scale of the data, HHT breaks down a signal into several intrinsic mode functions (IMFs) via empirical mode decomposition (EMD), and then calculates the instantaneous frequency of each IMF at any point in time via Hilbert transform. Hence, it is suitable for nonlinear and non-stationary data analysis. HHT has been broadly applied in numerous scientific disciplines and investigations, e.g., analysis on the bioelectricity signal, failure testing, and earthquake signals, etc [20]. Several researchers have applied HHT to EMG related studies. Xie et al. [18] and Peng et al. [21] adopted HHT to find the features of muscular fatigue. Ma and Luo [20] proposed using HHT and AR-model to extract the surface EMG feature to recognize hand-motions. Wang et al. [22] presented a feature extraction technique based on EMD to classify the walking activities from accelerometry data. Chen et al. [23] employed HHT to extract the frequency features of the stump to control transfemoral prosthesis. Zong and Chetouani [17] presented a feature extraction technique based on HHT for emotion recognition from physiological signals. In our previous research [24], we employed the EMD method to extract the upper-limb EMG signals for governing 1-DOF robot arms in real time.

This paper proposes developing an upper-limb EMG-based robot control system that can govern human assisting robot manipulators in natural and intuitive manner. The developed system is not intended to serve as a classifier that accurately identifies human intention from EMG signals. The development of such a classifier needs to well consider the influence from the muscle type, strength of muscle contraction, fatigue level, strategy in performing the task, and others. Instead, we attempt to develop a system for effective robot motion governing in real-time. At the current stage, we aim to govern the robot manipulator of 2 DOFs via the EMG signals measured from four surface electrodes placed on Biceps Brachii, Triceps Brachii, Pectoralis Major, and Teres Minor of the human operator. To tackle the non-stationary and nonlinear EMG signals generated during multi-joint movements, the EMD method is employed to break down the EMG signals into a set of IMFs, representing different physical characteristics for muscular movement recognition. We then utilize the initial point detection method previously proposed [10] to establish the relationship between the upper-limb EMG signals and corresponding robot arm movements in real time. As the selection of critical values in the initial point detection method is user-dependent, we need to find proper system parameters that are better suited for individual users. For such system parameter search, the adaptive neuro-fuzzy inference system (ANFIS) [10, 25] is employed to realize the fuzzy system, due to high complexity exhibited by the 2-DOF movements. A series of experiments are performed to demonstrate the effectiveness of the proposed system. Some other learning schemes have been proposed for related applications. Chan et al. [26] proposed a fuzzy approach to classify single-site EMG signals for prosthesis control based on the time-segmented features, which uses the Basic Isodata algorithm to cluster the features without supervision and the back-propagation algorithm to train the fuzzy rules. Vachkov and Fukuda [27] proposed structured learning and decomposition of fuzzy models for robotic control. The random walk algorithm with variable step size was used to tune the antecedent parameters of the membership functions and a local learning algorithm to tune the consequent parameters of the singletons.

The rest of the paper is organized as follows. In Section 2, the upper-limb EMG-based robot control system is described, including the modules for

EMG signal measurement and processing, EMD feature extraction, and motion classification with adaptation. Section 3 presents the experimental results and discussions. The conclusion is given in Section 4.

2 Proposed Upper-Limb EMG-Based Robot Control System

Figure 1 shows the system diagram of the proposed upper-limb, EMG-based robot control system for governing a 2-DOF robot manipulator, which consists of three main modules: signal measurement and processing, EMD feature extraction, and motion classification with adaptation. The signal measurement and processing module measures the raw EMG signals and also filters out noise. The filtered EMG signals are then sent to the EMD feature extraction module to break down the signals into a set of IMFs. With the IMFs, the motion classification with adaptation module then determines the arm movement of the operator and generates the commands to drive the human-assisting robot. From the resultant robot motion, the operator evaluates the performance and determines the next movement. These three modules are described below.

2.1 Signal Measurement and Processing

For this upper-limb, EMG-based robot control system, we extract the EMG signals of Biceps Brachii, Triceps Brachii, Pectoralis Major, and Teres Minor. To obtain more precise EMG signals, the electrodes are placed on the belly of the muscle. The recommended inter-electrode distance (from one differential electrode to the other) is about 1∼2 cm [28, 29]. Several types of noises may affect the measurement of the EMG signals, such as ECG crosstalk, electromagnetic induction from power lines, and arm and cable movements. The ECG crosstalk can be suppressed by measuring signals from those muscles away from the heart. The frequency of the electromagnetic noise is around 60 Hz. While a notch filter at that frequency can be an option, it should be avoided, because EMG generates many extra signals at these and neighboring frequencies (the primary frequency of the EMG signal is 50∼150 Hz). We thus let the proposed approach tackle its influence as the disturbance. Meanwhile, the frequency distribution for the arm and cable movements is around 0–20 Hz, which can be handled using a high-pass filter.

2.2 Empirical Mode Decomposition Feature Extraction

Hilbert–Huang transform (HHT) [21, 23, 30] is an adaptive signal processing technique based on the local characteristic time scale of the data. The key part of the HHT is the EMD process, which uses the sifting process to break down a complicated signal without a basis function, such as sine or wavelet functions, into several IMFs that are embedded in the complicated signal [31]. Each IMF, linear or nonlinear, represents a simple oscillation, which has the same number of extremes and zero-crossings. Figure 2 shows the flow chart of the

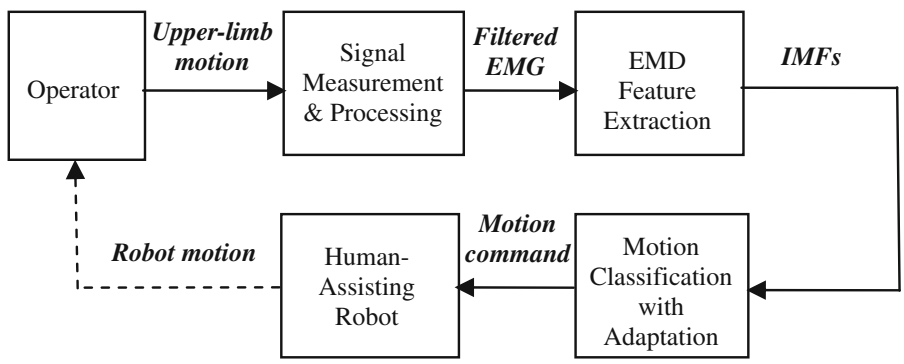

Fig. 1 Proposed upper-arm EMG-based robot control system

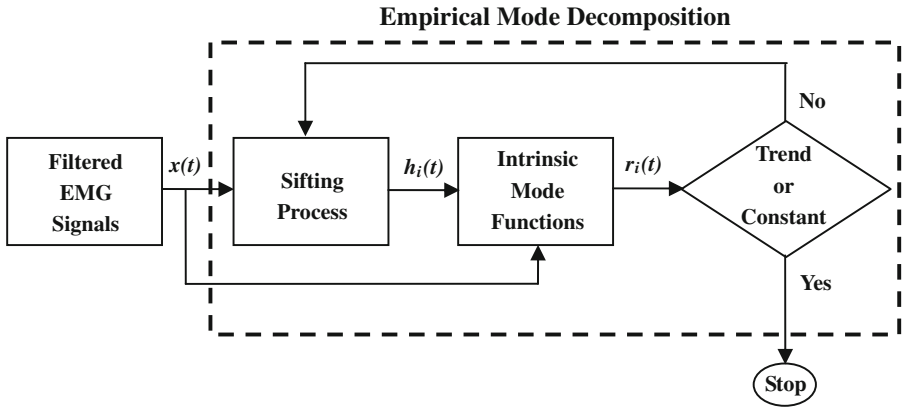

Fig. 2 Flow chart for empirical mode decomposition

EMD process, which breaks down the complete signal into a set of IMFs in eight steps:

Step 1 Obtain the upper envelop $U(t)$ of the filtered EMG data $x(t)$ by using a cubic spline curve to interpolate between those maximum points.

Step 2 Apply the same actions in Step 1 to obtain the lower envelope $L(t)$.

Step 3 Compute the mean value of the upper and lower envelope $m_1(t)$:

$$m_1(t) = \frac{U(t) - L(t)}{2} \tag{1}$$

Step 4 Subtract the running mean value $m_1(t)$ from the original data $x(t)$ to obtain the first component $h_1(t)$:

$$h_1(t) = x(t) - m_1(t) \tag{2}$$

Step 5 Iterate Steps 1–4 on $h_1(t)$ for k times

$$\begin{aligned} h_{11}(t) &= h_1(t) - m_{11}(t) \\ &\bullet \\ &\bullet \\ h_{1k}(t) &= h_{1(k-1)}(t) - m_{1(k-1)}(t) \end{aligned} \tag{3}$$

until the resulting component $h_{1k}(t)$ satisfies two conditions: (a) the difference between the number of local extremes and that of zero-crossings is zero or one and (b) the running mean value is zero. In Eq. 3, $m_{1(k-1)}(t)$ is the mean value of the upper and lower envelope of $h_{1(k-1)}(t)$.

Step 6 Designate $c_1(t) = h_{1k}(t)$ if h_{1k} meets the two requirements mentioned above.

Step 7 Subtract the first IMF $c_1(t)$ from the original data to obtain the residual $r_1(t)$:

$$r_1(t) = x(t) - c_1(t) \tag{4}$$

Step 8 Treat $r_1(t)$ as the new data and repeat Steps 1–7 on $r_1(t)$ to obtain all the subsequent i.e., $r_2(t) = r_1(t) - c_2(t), \ldots,$ $r_n(t) = r_{n-1}(t) - c_n(t)$ until the final residual $r_n(t)$ meets the predefined stopping criteria as a monotonic function, considered as the trend.

Based on the procedure above, the original data $x(t)$ can be exactly reconstructed by a linear superposition:

$$x(t) = \sum_{i=1}^{n} c_i(t) + r_n(t) \tag{5}$$

where n is the number of IMFs.

The number of IMFs depends on the characteristics of the data. Complex data can be decomposed into more IMFs, which increases the computational load in EMD. As EMG signals are nonlinear, non-stationary, and varying, using a high data sampling window would lead to a situation where the mapping between the upper-limb EMG signals and corresponding robot arm movements cannot be established within the expected time interval. After several experiments, it was found that combining a sixth-order band-pass Butterworth filter (a type of filter designed to have as flat a frequency response as possible in the passband) with the cut-off frequencies at 20 and 400 Hz with a window containing 20 samples

per second could reduce the computational load and noises, and this was used afterward. Figure 3 shows a typical example of the EMD process when a muscle relaxes and then flexes. Each of example includes the empirical EMG signal $x(t)$, three IMFs $(c_1(t), c_2(t), c_3(t))$, and residue $(r_3(t))$. Judging from Fig. 2a and b, $c_1(t)$ should be the background noise induced by skin impedance and temperature, cable movement, etc., since its magnitude did not vary with arm movement evidently. In contrast, those of $c_2(t)$ and $c_3(t)$ did vary. We found that the variation of the magnitude of $c_2(t)$

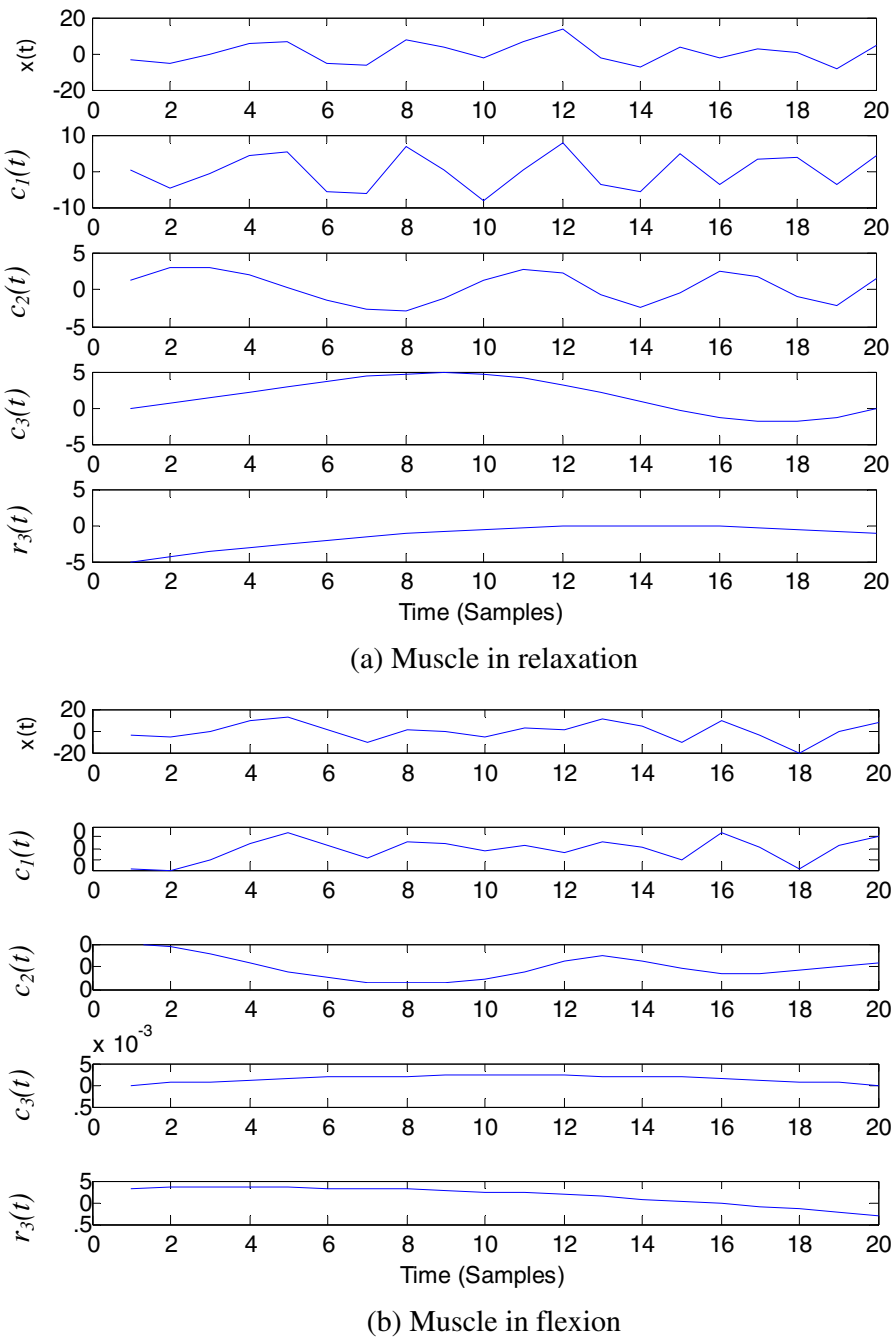

(a) Muscle in relaxation

(b) Muscle in flexion

Fig. 3 A typical example of an empirical EMG signal and corresponding empirical mode decomposition components, including 3 IMFs and 1 residue (trend): muscle in **a** relaxation and **b** flexion

is incremental, which basically followed that of the muscle activities, while that of $c_3(t)$ is decremental. Therefore, $c_2(t)$ was identified to represent the limb movement.

2.3 Motion Classification with Adaptation

To achieve real-time motion classification, we adopt the initial critical value detection method previously proposed. Note that this method is not intended to provide a classifier that accurately identifies human intention from EMG signals, but to efficiently establish the relationship between the upper-limb EMG signal and corresponding movements. Its feasibility and effectiveness have been verified via experiments based on one-joint upper-limb movement [10, 24]. Details of the method can be referred to [10, 24], and are briefly described below.

The initial point detection method determines the onset of the upper limb motion by detecting the instant when the magnitude of the extracted feature reaches the critical value, as illustrated in Fig. 4. In Fig. 4, the state of the muscle, *MS*, is determined to be active when the value for the extracted feature F_k, calculated by the root mean square (RMS) method, is larger than the predefined upper critical value CV_u, and MS is inactive when F_k is smaller than the predefined lower critical value CV_l. Furthermore, an active *MS* corresponds to an "ON" robot command and an inactive one to "OFF." This relationship can be formulated as:

$$MS = \begin{cases} 1, \; if \; F_k > CV_u \\ 0, \; if \; F_k < CV_l \end{cases} \tag{6}$$

where $F_k = RMS(c_2(t))$, $0 \leq t \leq 20$ samples, and $c_2(t)$ is the 2nd IMF.

The proper selection of CV_u and CV_l is critical for the performance of the motion classifier. And, their selection is user-dependent. Finding the proper CV_u and CV_l for individual users is very challenging, especially when limb movements of multi-DOF are involved. In the search of proper CV_u and CV_l, we employ the adaptive neuro-fuzzy inference system (ANFIS) [25] to utilize the fuzzy system due to its excellence at adaptation. Figure 5 shows the conceptual diagram of the proposed ANFIS for CV_u and CV_l determination, which consists of fuzzy rule, fuzzifier, fuzzy inference engine, and defuzzifier. We utilize the empirical knowledge to generate the fuzzy rules, listed in Table 1, where IN_a, IN_b, IN_c, and IN_d stand for the EMG signals of BB, TB, PM, and TM, respectively, OUT for CV_u, and W, M, S, VL, L, H, and VH for weak, middle, strong, very low, low, high, and very high. Fuzzifier transforms the measured EMG signals of Biceps Brachii (BB), Triceps Brachii (TB), Pectoralis Major (PM), and Teres Minor (TM) into linguistic variables. In addition, a one-degree Sugeno-type inference system is employed to depict the fuzzy rules in the fuzzy inference engine. The fuzzy rules are formulated as:

$$\begin{aligned} R^i: \; & IF \; \text{BB} \; is \; A_i \; and \; \text{TB} \; is \; B_i \; and \; \text{PM} \; is \; C_i \\ & and \; \text{TM} \; is \; D_i \; THEN \; CV_u \; (CV_l) \\ & = p_i \times \text{BB} + q_i \times \text{TB} + r_i \times \text{PM} + s_i \\ & \times \text{TM}, \; i \in \{1, \; 2, \; \ldots, 54\} \end{aligned} \tag{7}$$

where BB, TB, PM, and TM are the input variables, A, $B, C, D = \{\text{W, M, S}\}$ the linguistic variables, $CV_u(CV_l)$ the output variable, and $[p_i \, q_i \, r_i \, s_i]$ the consequent parameter set, which can be determined by the least-squares method. Defuzzifier transforms the fuzzy results of the inference into a real $CV_u(CV_l)$ using the weighted averaged method.

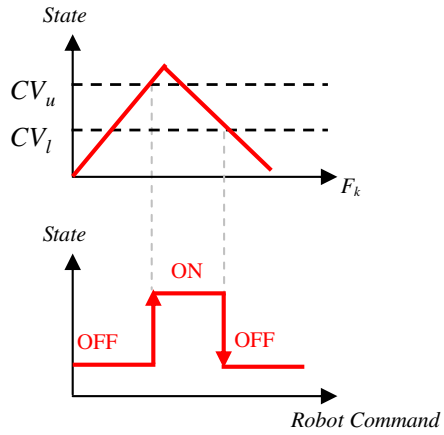

Fig. 4 Conceptual diagram for initial value detection

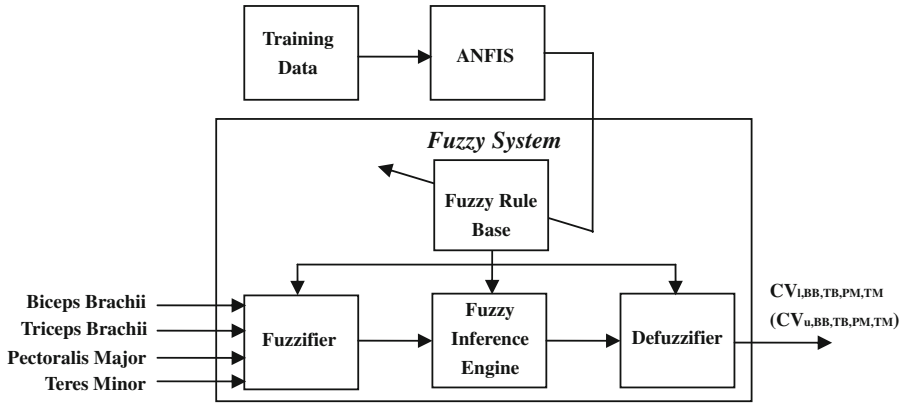

Fig. 5 Conceptual diagram of the proposed ANFIS to determine CV_u and CV_l

Via extensive experiments, the values of the W, M, and S in $IN_a \sim IN_d$ and those of VL, L, M, H and VH in OUT are empirically set, as shown in Table 2, and CV_l is set to be 0.7 times the value of CV_u. Since some conditions, such as skin impedance and temperature, etc. may be different from those for training, the values aforementioned can be adjusted via a compensating factor λ, ranging from 0.8 to 1.3. The procedure for determining CV_u and CV_l is described as follows:

Step 1 Set the compensating parameter λ to be 0.8 in the proposed ANFIS to obtain the first set of CV_u and CV_l.

Step 2 Ask the operator to perform the motion of flexion, extension, internal rotation,

Table 1 Fuzzy rule base

Rule No.	IN_a	IN_b	IN_c	IN_d	OUT	Rule No.	IN_a	IN_b	IN_c	IN_d	OUT
1	W	W	W	W	VL	28	M	W	W	W	L
2	W	W	W	M	VL	29	M	W	W	M	L
3	W	W	W	S	L	30	M	W	W	S	M
4	W	W	M	W	VL	31	M	W	M	W	L
5	W	W	M	M	L	32	M	W	M	M	M
6	W	W	M	S	L	33	M	W	M	S	M
7	W	W	S	W	VL	34	M	W	S	W	L
8	W	W	S	M	L	35	M	W	S	M	M
9	W	W	S	S	L	36	M	W	S	S	M
10	W	M	W	W	L	37	M	M	W	W	M
11	W	M	W	M	L	38	M	M	W	M	M
12	W	M	W	S	L	39	M	M	W	S	M
13	W	M	M	W	M	40	M	M	M	W	H
14	W	M	M	M	M	41	M	M	M	M	H
15	W	M	M	S	M	42	M	M	M	S	H
16	W	M	S	W	M	43	M	M	S	W	H
17	W	M	S	M	M	44	M	M	S	M	H
18	W	M	S	S	M	45	M	M	S	S	H
19	W	S	W	W	H	46	M	S	W	W	VH
20	W	S	W	M	H	47	M	S	W	M	VH
21	W	S	W	S	H	48	M	S	W	S	VH
22	W	S	M	W	H	49	M	S	M	W	VH
23	W	S	M	M	H	50	M	S	M	M	VH
24	W	S	M	S	H	51	M	S	M	S	VH
25	W	S	S	W	VH	52	M	S	S	W	VH
26	W	S	S	M	VH	53	M	S	S	M	VH
27	W	S	S	S	VH	54	M	S	S	S	VH

Table 2 Values of the linguistic variables in the fuzzy rule base

$IN_a \sim IN_d$			OUT				
W	M	S	VL	L	M	H	VH
1/3	2/3	1	1/3	2/3	1	4/3	5/3

and external rotation two times consecutively.

Step 3 If the successful discrimination rate (SDR), defined in Eq. 8 below, is lower than 80%, add 0.1 to λ, and iterate Steps 2 and 3 until the SDR is equal to or more than 80%.

$$SDR = \frac{Number\ of\ successful\ motions\ following}{Total\ number\ of\ classifications} \times 100\% \quad (8)$$

The proposed ANFIS consists of five layers, as shown in Fig. 6. Layer 1 is the input layer. Each

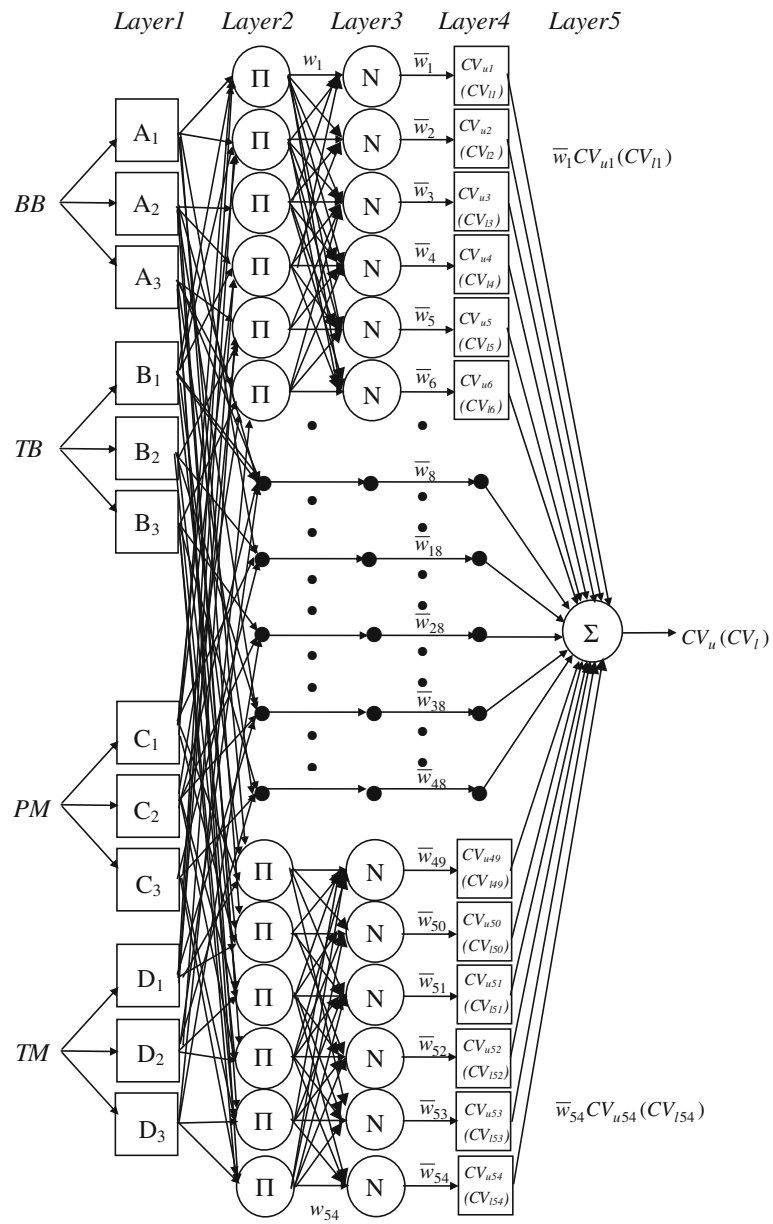

Fig. 6 Structure of the ANFIS for the proposed system

node in this layer represents an input variable of the model with the membership function:

$$O_i^1 = \mu_{A_i}(BB),\ O_{i+3}^1 = \mu_{B_i}(TB),$$
$$O_{I+6}^1 = \mu_{C_i}(PM),\ O_{i+9}^1 = \mu_{D_i}(TM),\ i = 1, 2, 3 \tag{9}$$

The bell-shaped membership function is employed, shown in Fig. 7, and is expressed as:

$$\mu_{Xi}(Y) = \frac{1}{1 + \left\{\left[(Y - c_i)/a_i\right]^2\right\}^{b_i}},\ i = 1, 2, 3 \tag{10}$$

where $[X, Y] \in \{[A, BB], [B, TB], [C, PM], [D, TM]\}$, $[a_i\, b_i\, c_i]$ represent the premise parameter set, which can be determined by the backpropagation gradient descent method. Layer 2 is the inference layer. Each node in this layer is multiplied by the input signal to become w_i:

$$O_i^2 = w_i = \mu_{Ai}(BB) \times \mu_{Bi}(TB) \times \mu_{Ci}(PM) \times \mu_{Di}(TM),\ i = 1, 2, \cdots, 54 \tag{11}$$

w_i stands for the firing strength of the rule. Layer 3 is the normalization layer that normalizes the firing strength by calculating the ratio of i^{th} firing strength to their sum:

$$O_i^3 = \overline{w}_i = \frac{w_i}{\sum_{j=1}^{54} w_j},\ i = 1, 2, \cdots, 54 \tag{12}$$

Layer 4 is the output layer. Each node multiplies the normalized firing strength by the consequent function to generate the qualified consequent of each rule. The output of the node is computed as:

$$O_i^4 = \overline{w}_i CV_u (CV_l)_i = \overline{w}_i (p_i BB + q_i TB + r_i PM + s_i TM),\ i = 1, 2, \cdots, 54 \tag{13}$$

Layer 5 is the defuzzification layer, which computes the weighted average of the output signals from the output layer:

$$O_i^5 = \sum_{i=1}^{54} \overline{w}_i CV_u (CV_l)_i = \frac{\sum_{i=1}^{54} w_i CV_u (CV_l)_i}{\sum_{i=1}^{54} w_i} \tag{14}$$

3 Experiments

We performed a series of experiments to evaluate the performance of the proposed system. Figure 8 shows the implementation of the proposed system for experiments. In Fig. 8, the measured EMG signals are first amplified using the ETH-256 physiological signal amplifier (manufactured by iWorx Systems, USA), and the amplified analog signals (voltages) then transformed into digital signals

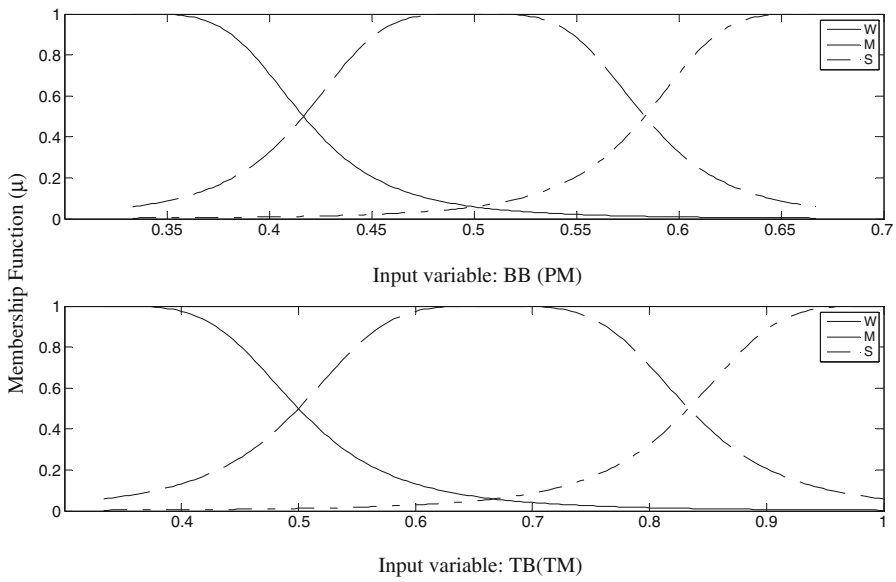

Fig. 7 Bell-shaped membership functions for input variables

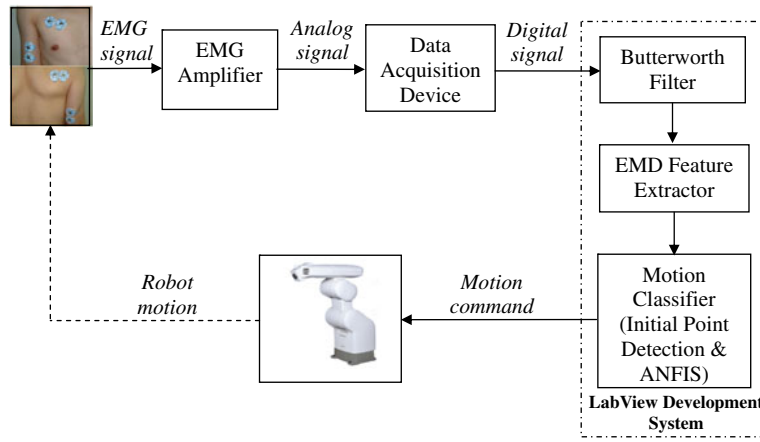

Fig. 8 System implementation of the proposed scheme

via a National Instrument USB-6009 A/D data acquisition device with a 1 KHz sampling rate. The digital signals are further forwarded to the LabVIEW development system, which includes a sixth-order band-pass Butterworth filter with the cut-off frequencies at 20 and 400 Hz, respectively, a 20-sampling-data-window EMD feature extractor; and a motion classifier with the initial point detector and ANFIS. By using this processing method, robot motion commands can be determined, and then sent to a 6-DOF Mitsubishi RV-2A robot manipulator for execution (with only J1 and J2 manipulated). The entire experimental setup is shown in Fig. 9.

Four sets of electrodes were placed on BB, TB, PM, and TM, as shown in Fig. 10. The classifier is designed to let the feature extracted from BB, TB, PM, and TM correspond to upper limb flexion, extension, internal rotation, and external rotation, respectively, and those for both BB and PM and both TB and TM together for flexion-internal rotation and extension-external rotation, respectively. Their muscle states will determine whether it is an up, down, turn-left, turn-right, up-left, or down-right movement. Due to some muscle crosstalk or imprecise feature identification, there may be some conflict movement decisions between the two muscles. Under such circumstances, the classifier will send out an error signal. Totally, there are eight outputs for the classifier: STOP, UP, DOWN, LEFT, RIGHT, UP-LEFT, DOWN-RIGHT, and ERROR. Table 3 summarizes the mapping from EMG to robot movement, and Fig. 11 illustrates the classification outputs of 1∼6 corresponding to the robot arm movements.

Fig. 9 Experimental setup

Two male and two female subjects (with their physical data listed in Table 4) were asked to perform the following two experiments: (1) the motions of flexion, extension, internal rotation, and external rotation for four times consecutively, and (2) the motions of flexion plus internal rotation and extension plus external rotation for three times consecutively. The first experiment was used to evaluate the capability of the proposed system to recognize those motions related to basically one set of muscles (BB and TB or PM and TM), while the second experiment was used to recognize the motions involving the interaction between muscles, which incurred larger mutual interferences.

Figure 12 shows the results for the first experiment, which includes the subjects' filtered raw

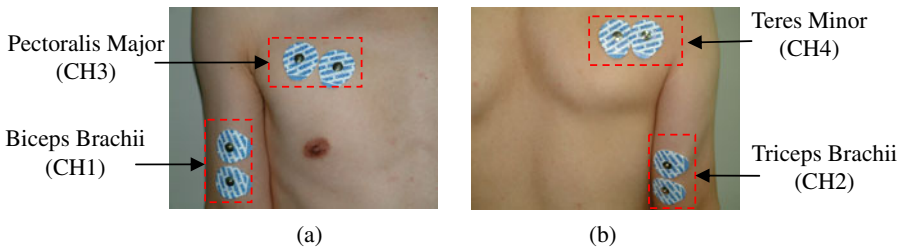

Fig. 10 Electrode locations: **a** Biceps Brachii and Pectoralis Major and **b** Triceps Brachii and Teres Minor

Table 3 Mapping from EMG to robot movement

EMG				Upper limb status	Classifier output	Robot arm
BB (CH1)	TB (CH2)	PM (CH3)	TM (CH4)			
OFF	OFF	OFF	OFF	Relaxation	0	STOP
ON	OFF	OFF	OFF	Flexion	1	J2 axis UP
OFF	**ON**	OFF	OFF	Extension	2	J2 axis DOWN
OFF	OFF	**ON**	OFF	Internal Rotation	3	J1 axis TURN LEFT
OFF	OFF	OFF	**ON**	External Rotation	4	J1 axis TURN RIGHT
ON	OFF	**ON**	OFF	Flexion-Internal Rotation	5	J1 axis TURN LEFT and J2 axis UP
OFF	**ON**	OFF	**ON**	Extension-External Rotation	6	J1 axis TURN RIGHT and J2 axis DOWN
All others				Error	7	STOP

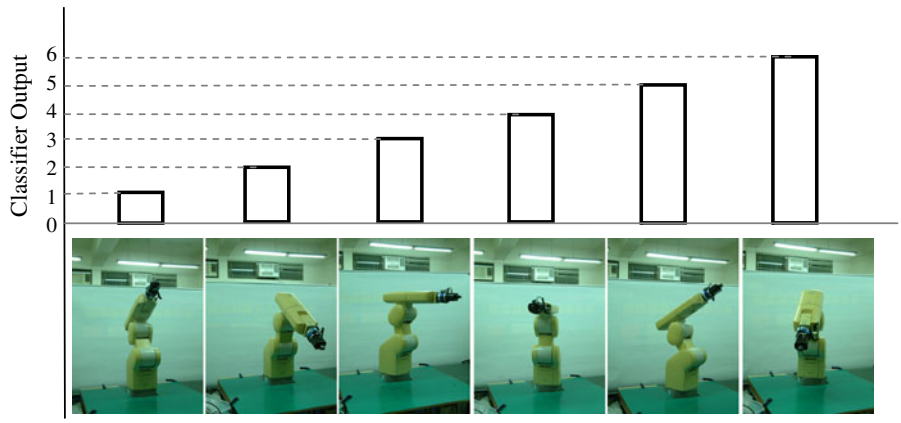

Fig. 11 Illustrations of classification outputs corresponding to the robot arm movements

Table 4 Physical data of the subjects

Subject	Height (cm)	Weight (kg)	Gender	Body type
A	166	60	Male	Slender
B	164	82	Male	Overweight
C	155	52	Female	Normal
D	150	50	Female	Normal

EMG signals, muscle states, and classification outputs. The muscle states reveal that subjects C and D exhibited certain muscle mutual interferences during movements, especially for subject D. The SDR for the subjects is 97%, 99%, 87.9%, and 81.8%, respectively. For these four kinds of motions dominated by basically one set of muscles, the proposed system achieved quite high a successful discrimination rate, even for subject D.

Figure 13 shows the results of the second experiment. Different from the motions executed in the first experiment, these motions involved the onsets of two muscles simultaneously, leading to larger mutual interferences and couplings between muscles. In Fig. 13, some muscle states of

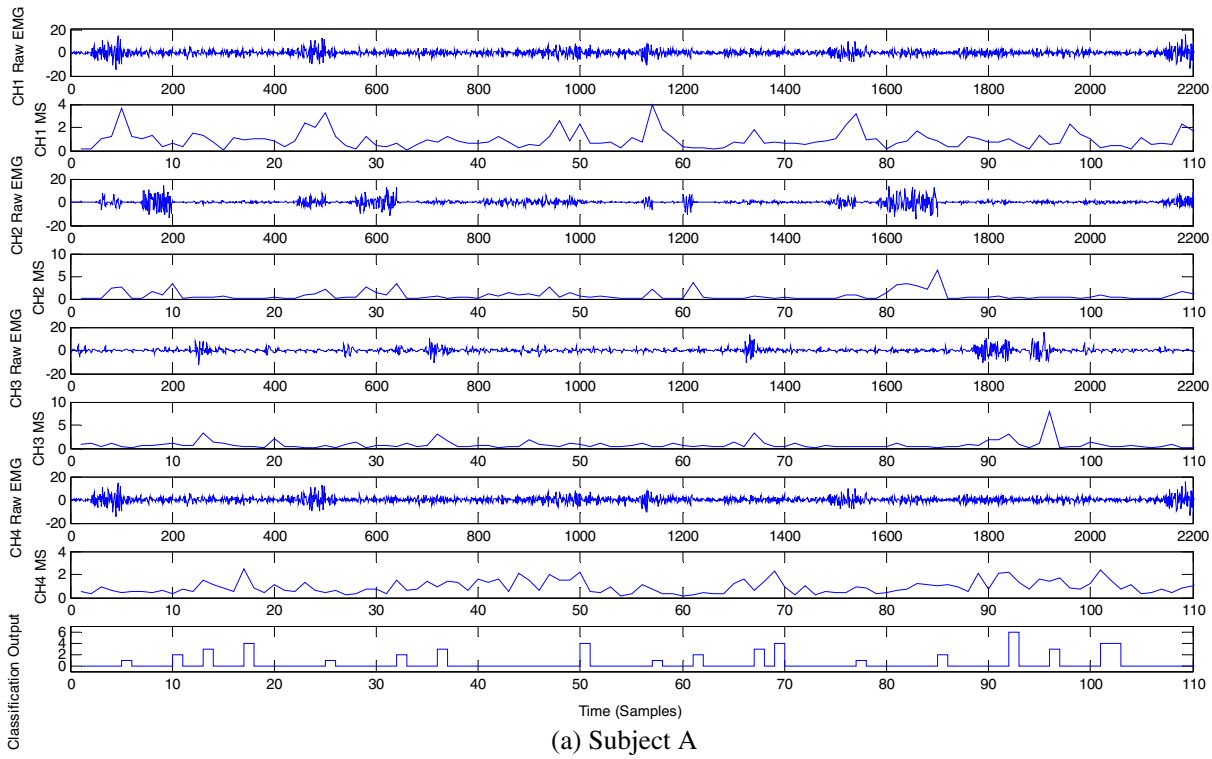

(a) Subject A

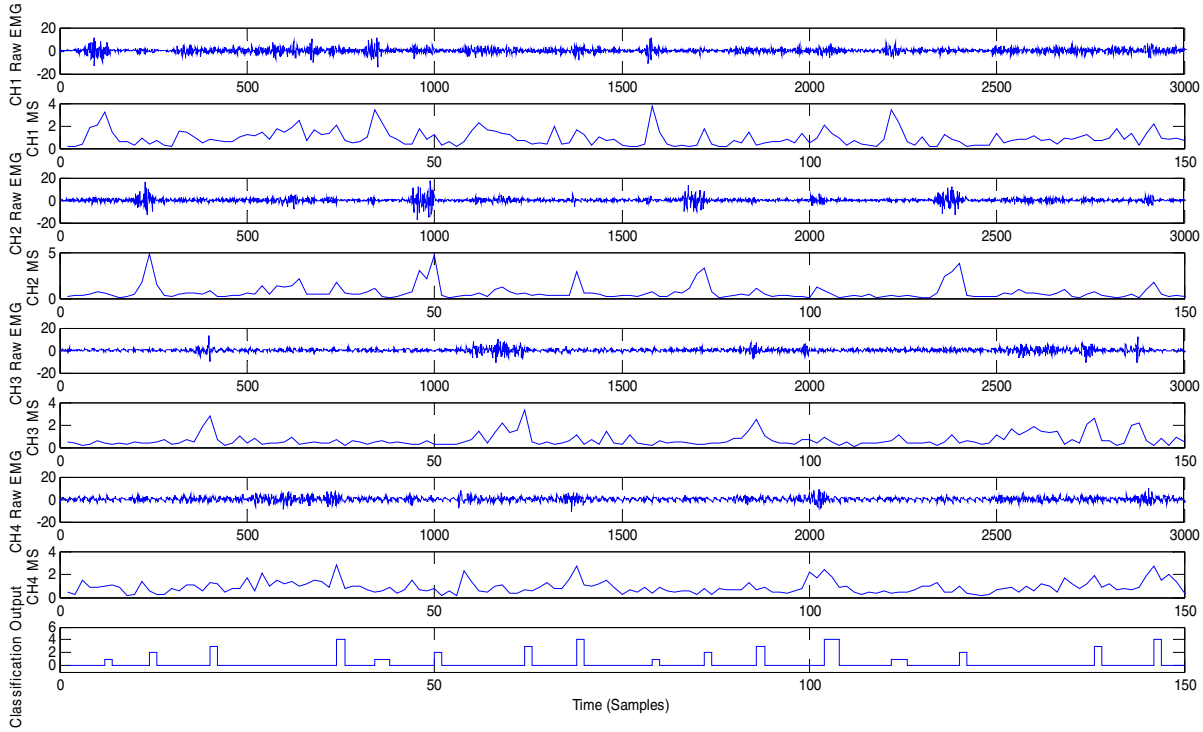

(b) Subject B

Fig. 12 Experimental results for the motions of flexion, extension, internal rotation, and external rotation for four times consecutively

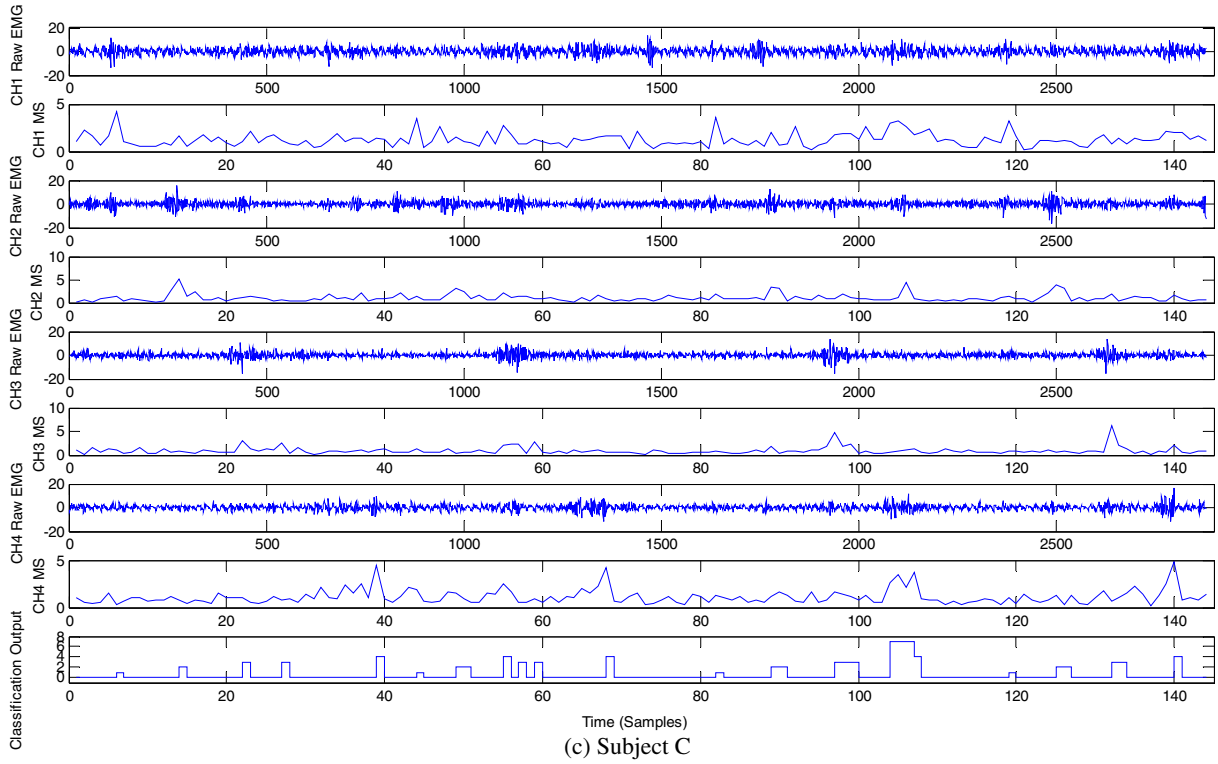

(c) Subject C

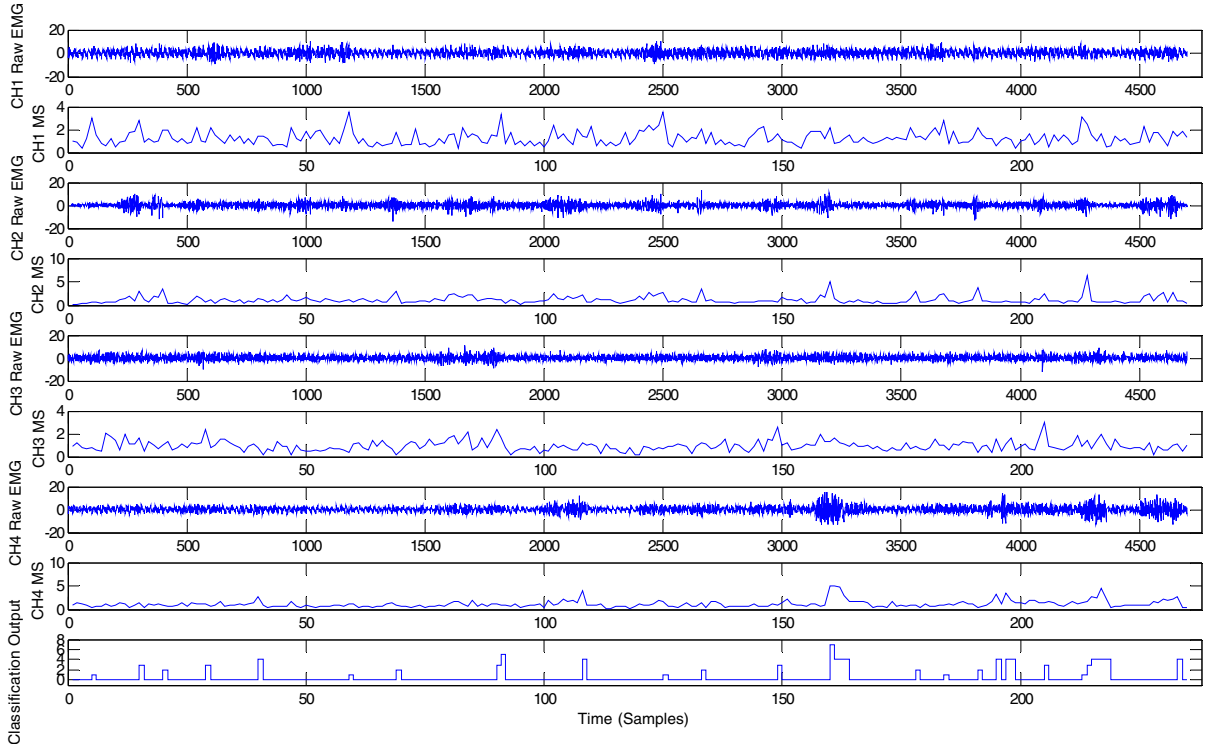

(d) Subject D

Fig. 12 (continued).

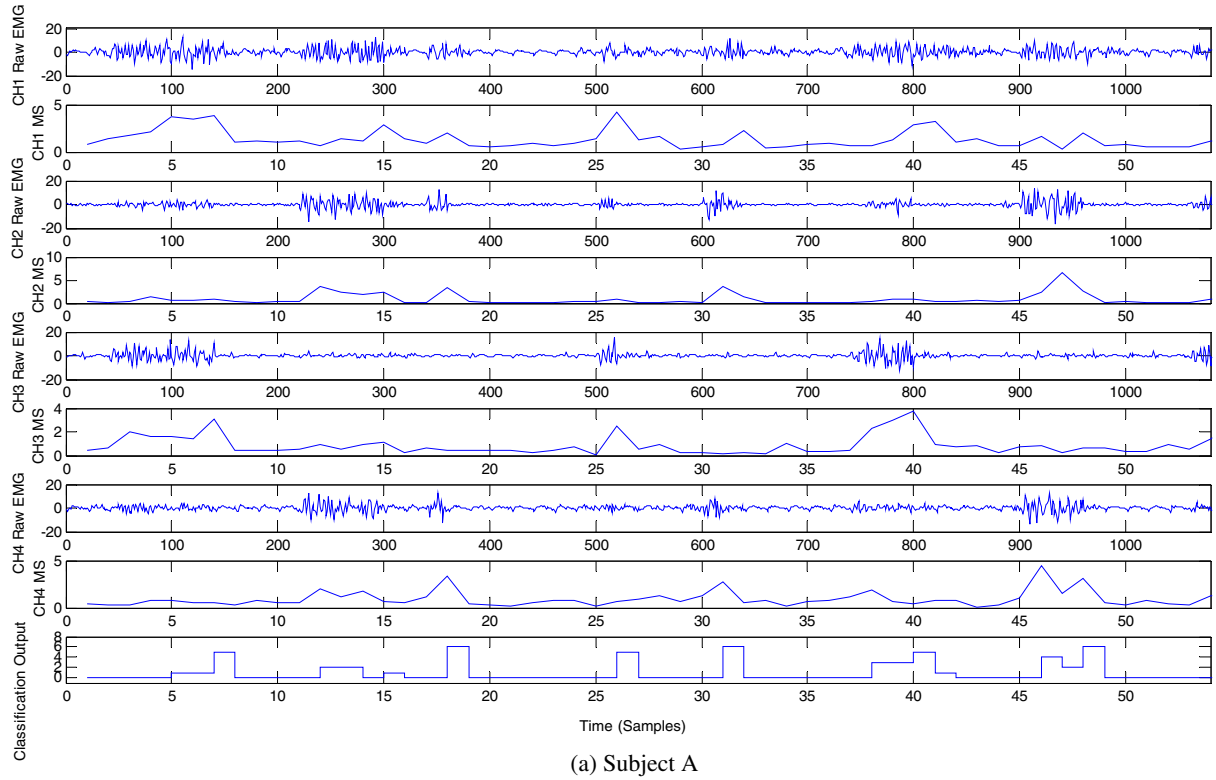

(a) Subject A

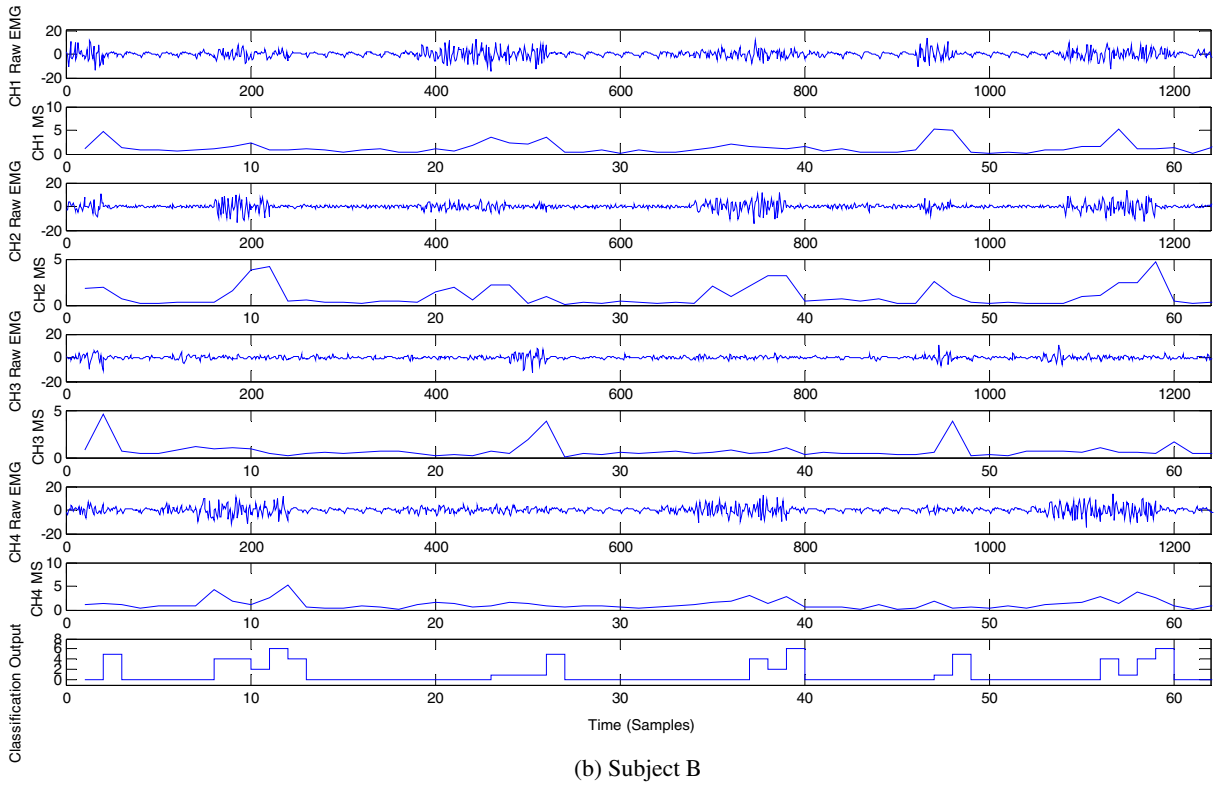

(b) Subject B

Fig. 13 Experimental results for the motions of flexion plus internal rotation and extension plus external rotation for three times consecutively

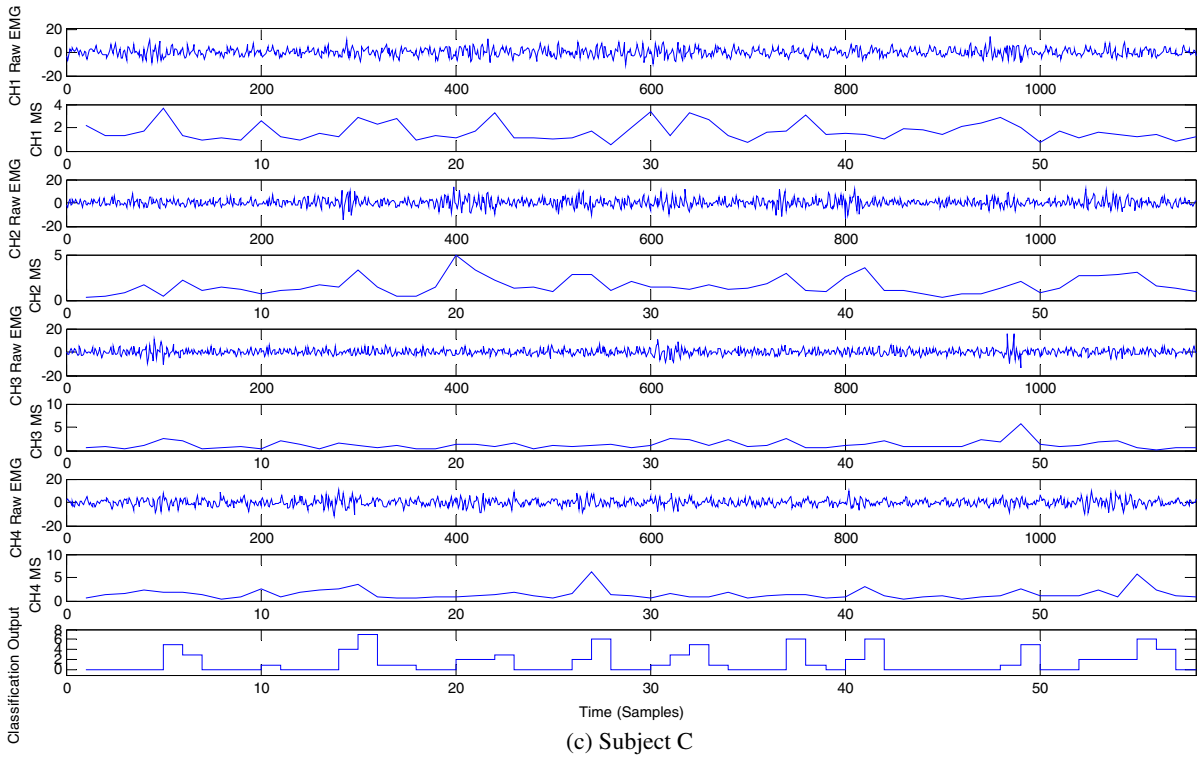

(c) Subject C

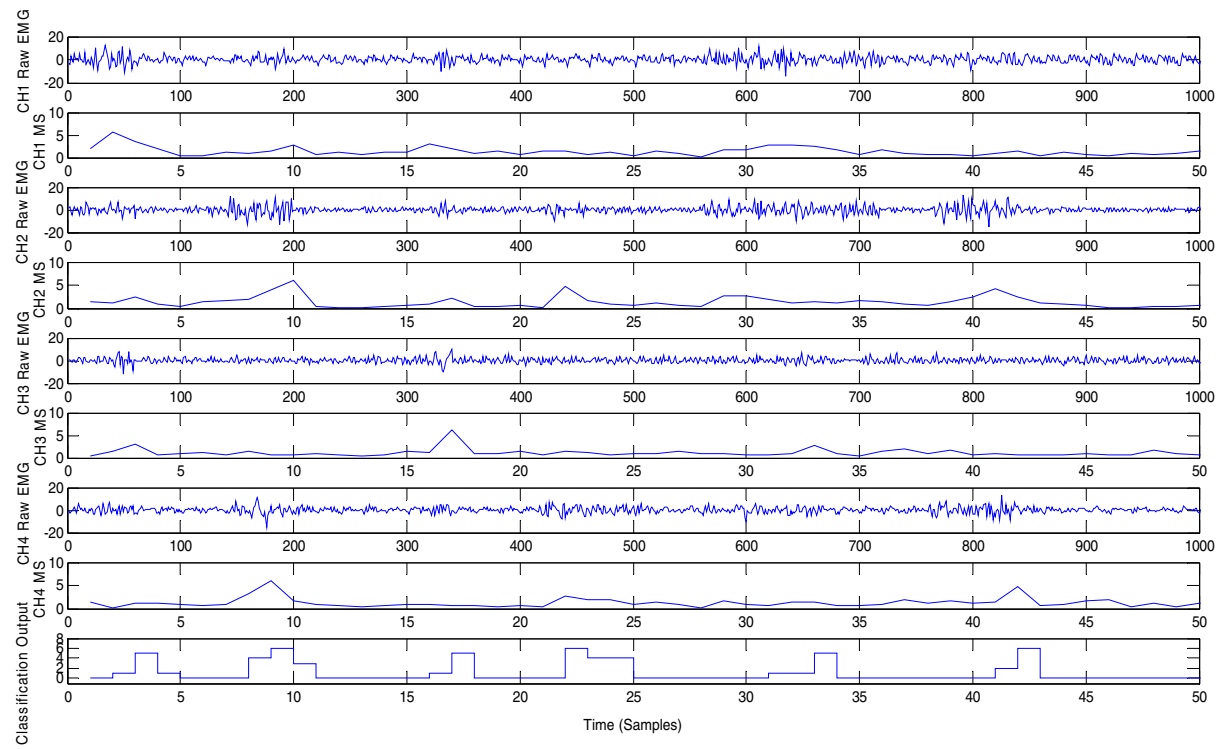

(d) Subject D

Fig. 13 (continued).

BB and PM (also TB and TM) did not simultaneously reach the individual critical upper value. However, the SDR for the subjects was found to be 84.6%, 92.3%, 76.9%, and 99%, respectively, indicating that the proposed system still managed these complex motions well. Videos for these experiments can be located via the link connected to our laboratory Web page (http://140.113.149.114).

4 Conclusion

This paper presents an upper-limb EMG-based robot control system for achieving natural and intuitive robot manipulation. By integrating the initial point detection method previously proposed with the EMD approach and the ANFIS, the mapping between the upper limb EMG signals and corresponding robot arm movements has been established in real-time. Experiments have been performed to demonstrate its effectiveness. For the potential user to apply the proposed system for movements involving upper or other limbs, or involving more DOFs, they can follow the proposed procedure, possibly at the expense of more sophisticated learning schemes to deal with the incurring complexity. In future works, we plan to investigate the possibility of using varying *CVs,* because fixed *CVs* lead to consistent classification for about 5∼10 min, depending on the status of muscle fatigue. Our intention is to let the system maintain a high successful discrimination rate for a longer time. We also plan to apply the proposed system for full limb movement governing.

Acknowledgements This work was supported in part by the National Science Council under grant NSC 99-2221-E-009-157, and also Department of Industrial Technology under grants 97-EC-17-A-02-S1-032.

References

1. Kermani, M.Z., Wheeler, B.C., Badie, K., Hashemi, R.M.: EMG feature evaluation for movement control of upper extremity prostheses. IEEE Trans. Rehabil. Eng. **3**(4), 324–333 (1995)
2. Huang, H.P., Chen, C.Y.: Development of a myoelectric discrimination system for a multi-degree prosthetic hand. In: IEEE International Conference on Robotics and Automation (1999)
3. Chen, L., Yang, P., Zu, L., Guo, X.: Movement recognition by electromyography signal for transfemoral prosthesis control. In: IEEE Conference on Industrial Electronics and Applications (2009)
4. Harada, A., Nakakuki, T., Hikita, M., Ishii, C.: Robot finger design for myoelectric hand and recognition of finger motions via surface EMG. In: IEEE Conference on Automation and Logistics (2010)
5. Fukuda, O., Tsuji, T., Kaneko, M., Otsuka, A.: A human-assisting manipulator teleoperated by EMG signals and arm motions. EEE Trans. Robot. Autom. **19**(2), 210–222 (2003)
6. Artemiadis, P.K., Kyriakopoulos, K.J.: EMG-based position and force control of a robot arm: application to teleoperation and orthosis. In: IEEE/ASME International Conference on Advanced Intelligent Mechatronics (2007)
7. Ferreira, A., Celeste, W.C., Cheein, F.A., Bastos-Filho, T.F., Sarcinelli-Filho, M., Carelli, R.: Human-machine interfaces based on EMG and EEG applied to robotic systems. J. Neuroeng. Rehabil. **5**(10), 1–15 (2008)
8. Gopura, R.A.R.C., Kiguchi, K.: EMG-based control of an exoskeleton robot for human forearm and wrist motion assist. In: IEEE International Conference on Robotics and Automation (2008)
9. Bu, N., Okamoto, M., Tsuji, T.: A hybrid motion classification approach for EMG-based human–robot interfaces using Bayesian and neural networks. EEE Trans. Robot. **25**(3), 502–511 (2009)
10. Liu, H.J., Young, K.Y.: An adaptive upper-arm EMG-based robot control system. Int. J. Fuzzy Syst. **12**(3), 181–189 (2010)
11. Li, Y., Tian, Y., Chen, W.: Multi-pattern recognition of sEMG based on improved BP neural network algorithm. In: Chinese Control Conference (2010)
12. Phinyomark, A., Hirunviriya, S., Limsakul, C., Phukpattaranont, P.: Evaluation of EMG feature extraction for hand movement recognition based on Euclidean distance and standard deviation. In: International Conference on Electrical Engineering/Electronics Computer Telecommunications and Information Technology (2010)
13. Meng, M., She, Q., Gao, Y., Luo, Z.: EMG signals based gait phases recognition using hidden Markov models. In: IEEE International Conference on Information and Automation (2010)
14. Gora, J., Szecowka, P.M., Wolczowski, A.R.: Control of dexterous hand—algorithm implementation issues. In: International Conference on Information Technology and Applications in Biomedicine (2009)
15. Karlsson, S., Yu, J., Akay, M.: Enhancement of spectral analysis of myoelectric signals during static contractions using wavelet methods. IEEE Trans. Biomed. Eng. **46**, 670–684 (1999)
16. Mahaphonchaikul, K., Sueaseenak, D., Pintavirooj, C., Sangworasil, M., Tungjitkusolmun, S.: EMG signal feature extraction based on wavelet transform. In: International Conference on Electrical Engineering/Electronics Computer Telecommunications and Information Technology (2010)

17. Zong, C., Chetouani, M.: Hilbert–Huang transform based physiological signals analysis for emotion recognition. In: IEEE International Symposium on Signal Processing and Information Technology (2009)
18. Xie, H., Wang, Z.: Mean frequency derived via Hilbert–Huang transform with application to fatigue EMG signal analysis. Comput. Methods Programs Biomed. **82**, 114–120 (2006)
19. Andrade, A.O., Nasuto, S., Kyberd, P., Sweeney-Reed, C.M., Van Kanijn, F.R.: EMG signal filtering based on empirical mode decomposition. Biomed. Signal Process Contr. **1**, 44–45 (2006)
20. Ma, W., Luo, Z.: Hand-motion pattern recognition of sEMG based on Hilbert–Huang transformation and AR-model. In: IEEE International Conference on Mechatronics and Automation (2007)
21. Peng, B., Jin, X., Min, Y., Su, X.: The study on the sEMG signal characteristics of muscular fatigue based on the Hilbert–Huang transform. In: International Conference on Computational Science (2006)
22. Wang, N., Ambikairajah, E., Celler, B.G., Lovell, N.H.: Accelerometry based classification of gait patterns using empirical mode decomposition. In: IEEE International Conference on Acoustics, Speech, and Signal Processing (2008)
23. Chen, L., Yang, P., Zu, L., Guo, X.: Movement recognition by electromyography signal for transfemoral prosthesis control. In: IEEE Conference on Industrial Electronics and Applications (2009)
24. Liu, H.J., Young, K.Y.: Robot motion governing using upper limb EMG signal based on empirical mode decomposition. In: IEEE International Conference on Systems, Man, and Cybernetics (2010)
25. Jang, J.S.R.: ANFIS: adaptive network based fuzzy inference system. IEEE Trans. Syst. Man Cybern. **23**(3), 665–683 (1993)
26. Chan, Francis H.Y., Yang, Y.S., Lam, F.K., Zhang, Y.T., Parker, P.A.: Fuzzy EMG classification for prosthesis control. In: IEEE Trans. Rehabil. Eng. **8**(3), 305–311 (2000)
27. Vachkov, G., Fukuda, T.: Structured learning and decomposition of fuzzy models for robotic control applications. J. Intell. Robot. Syst. **32**(1), 1–21 (2001)
28. Luca, C.J.D.: The use of surface electromyography in biomechanics. J. Appl. Biomech. **13**(2), 135–163 (1997)
29. Henryk, K., Grzegorz, S., Anton, N.: Effect of electrode position on EMG recording in pectoralis major. J. Hum. Kinet. **17**, 105–112 (2007)
30. Huang, N.E., Zhen, S., Long, S.R., Wu, M.C., Shin, H.H., Zheng, Q., Yen, N.C., Tung, C.C., Liu, H.H: The empirical mode decomposition and the Hilbert spectrum for nonlinear and non-stationary time series analysis. Proc. R. Soc. Lond. **454**(A), 903–995 (1998)
31. Li, X., Li, D., Liang, Z., Voss, Z.J., Sleigh, J.W.: Analysis of depth of anesthesia with Hilbert–Huang spectral entropy. Clin. Neurophysiol. **119**(11), 2465–2475 (2008)